Proton total reaction cross sections for ^{42}Ca, ^{44}Ca, and ^{48}Ca between 21 and 48 MeV

R. F. Carlson and A. J. Cox
Department of Physics, University of Redlands, Redlands, California 92373

N. E. Davison, T. Eliyakut-Roshko, R. H. McCamis,* and W. T. H. van Oers
Cyclotron Laboratory, Department of Physics, University of Manitoba, Winnipeg, Manitoba, Canada R3T 2N2
(Received 19 January 1994)

Proton total reaction cross sections (σ_R) have been measured for the nuclei ^{42}Ca, ^{44}Ca, and ^{48}Ca at seven energies each between 20.8 and 48.0 MeV. The experimental results plus our previously measured σ_R values for ^{40}Ca are compared to the results of optical model analyses, both nonrelativistic and relativistic, of an extensive set of elastic scattering data for the same calcium isotopes in this energy range. The experimental results are also compared to global optical model predications. In general, the theoretical values are in good agreement with the experimental results, with a slight preference for the relativistic analysis. In addition, our results are used in nuclear transparency calculations, which show that over the range of energies studied, the average nuclear transparency decreases by almost 15%.

PACS number(s): 25.40.−h, 24.10.Ht, 27.40.+z

I. INTRODUCTION

A series of experiments was undertaken to measure proton elastic scattering and total reaction cross sections for a series of calcium nuclei ^{40,42,44,48}Ca in the energy range between 20 and 50 MeV. This series is particularly interesting since it both begins (^{40}Ca: Z=20 and N=20) and ends (^{48}Ca: Z=20 and N=28) with doubly magic nuclei.

In this energy range previous proton elastic scattering studies of calcium have been mainly confined to ^{40}Ca [1–10], although Austin *et al.* [11] have reported ratios of the differential cross sections for three of the calcium isotopes ^{40,44,48}Ca.

The present series of experiments began with measurements of the differential cross sections for protons on ^{42,44,48}Ca for mean proton energies of 21.0, 25.0, 30.0, 35.0, 40.0, 45.0, and 48.4 MeV and for protons on ^{40}Ca for energies of 25.0, 27.5, 30.0, 35.0, 40.0, and 45.0 MeV [12]. (Previous differential cross section measurements of p + ^{40}Ca had been made at 21.0, 23.5, 26.3, and 48.0 MeV by Bray *et al.* [5].) Optical model analyses of these data using both relativistic and nonrelativistic approaches have been reported [12], and differences between the rms radii of the neutron and proton distributions were deduced.

At energies below 500 MeV proton reaction cross sections had previously been measured for only one calcium isotope ^{40}Ca. Dicello and Igo [13] measured p+^{40}Ca σ_R in the energy range 10–22 MeV, and Turner *et al.* [14] reported a single measurement at 28.5 MeV. In an earlier experiment [15] our group measured σ_R at incident proton energies of 24.9, 30.0, 35.0, 40.0, 45.0, and 48.0 MeV for ^{40}Ca. At the proton energy of 700 MeV there are σ_R measurements on ^{40}Ca, ^{44}Ca, and ^{48}Ca [16].

In this paper, we report measurements and analyses of proton total reaction cross sections for ^{42}Ca and ^{44}Ca at incident energies of 20.8, 24.8, 29.7, 34.8, 39.7, 44.9, and 47.8 MeV and for ^{48}Ca at incident energies of 23.0, 25.3, 30.3, 35.1, 39.9, 45.3, and 48.0 MeV. The following sections of the paper describe the experimental method and the data reduction procedure. The experimental results are then presented and compared to a nuclear transparency calculation and to predictions from a global set of optical model parameters (nonrelativistic) as well as to relativistic and nonrelativistic optical model analyses of proton-calcium elastic scattering data.

II. EXPERIMENTAL METHOD

The experiment was performed using an attenuation technique [17]. A tightly collimated, momentum analyzed proton beam of energy known to ±150 keV F.W.H.M. from the University of Manitoba sector-focused cyclotron was incident on the total reaction cross section apparatus, a schematic drawing of which is shown in Fig. 1. Individual protons in the incident beam were detected by plastic scintillation detectors 1 and 2, with a coincidence requirement to aid in removing background. Protons entering the apparatus off axis or scattered by detectors 1 or 2 triggered one or both of the annular plastic scintillator detectors 3 and 4. Hence the trigger signal $12(\overline{3+4})$, the number of which is denoted I_0, indicated that a well-collimated proton was incident upon the target. After passing through the target, most protons or reaction products entered the stopping detector telescope, composed of the small plastic disk scintillator detector 5 and the CsI(Na) stopping detector 6. All

*Present address: Atomic Energy of Canada Limited, Pinawa, Manitoba, Canada R0E 1L0.

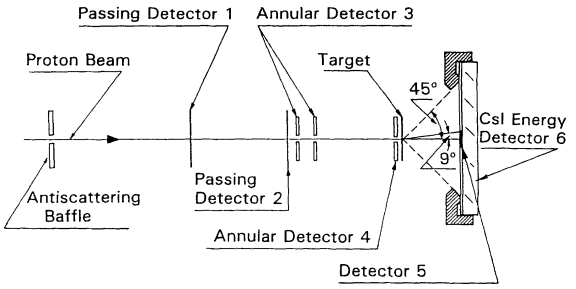

FIG. 1. Schematic diagram of the total reaction cross-section apparatus.

charged particles which entered detector 5 or deposited energy in detector 6 above the (E_{max} − 6.0 MeV) threshold (corresponding to elastic events plus, depending on the particular nucleus, a few inelastic states, and a small fraction of the continuum) produced an OR signal (5+6). The presence of an OR signal indicated a nonattenuation event I, which in most cases was an unscattered proton, but which also could have been an elastically scattered proton which entered detector 6 or a charged reaction product which entered detector 5. The OR signal I was placed in anticoincidence with the trigger signal I_0, directly yielding the difference $(I_0 - I)$, which corresponded to the number of attenuation events. In this manner the number of attenuation events was counted directly. The quantity $(I_0 - I)$ can be related to the total reaction cross section after applying a number of corrections which are described in Sec. III.

The experiment consisted of a series of "target in" and "target out" measurements at each of the several energies spanning the energy range of 20.8–47.8 MeV. For each target in or target out measurement the number of attenuation events for 10^7 trigger events was measured. Each measurement was repeated two or three times, and if any of the results were more than two standard deviations from the average, the measurements were repeated. As an illustration of a sample set of data at 44.9 MeV, for example, we measured 5686, 5649, and 5736 $(I_0 - I)$ events, each for 10^7 I_0 events for ^{42}Ca, and 6087, 6109, and 5996 for ^{44}Ca, while for the targets out we measured 970, 941, and 1012 $(i_0 - i)$ events, each for 10^7 i_0 events. A more detailed description of the experimental technique is given in Ref. [17].

Circular solid targets of ^{42}Ca, ^{44}Ca, and ^{48}Ca were fabricated by Isotope Sales, ORNL. The highly oxidizable targets were weighed prior to the experiment in an airtight glove box filled with an inert gas and then transferred to the airtight target holding apparatus. After completion of the experiment (under vacuum) the targets were weighed again in the glove box to determine the mass of any added contaminant, which was found to be less than 0.2%. Target characteristics are given in Table I.

TABLE I. Target characteristics.

Target	ρx (g/cm^2)	Enrichment (%)
^{42}Ca	0.0392±0.000 6	93.71
^{44}Ca	0.0424±0.000 7	98.68
^{48}Ca	0.0104±0.000 25	90.81

III. DATA REDUCTION

The uncorrected cross section σ_{un} was calculated using the formula

$$\sigma_{un} = \frac{1}{nx}\left[\frac{(I_0 - I)}{I_0} - \frac{(i_0 - i)}{i_0}\right],$$

where $(I_0 - I)$ and $(i_0 - i)$ are the number of attenuation events with target in and out, respectively, while I_0 and i_0 are the number of trigger protons $12(\overline{3+4})$ with target in and out, respectively, and nx is the number of nuclei per cm^2 in the target.

The total reaction cross section σ_R was obtained from σ_{un} by applying corrections for the following effects.

(i) Elastic scattering events. Protons scattered at angles greater than 45° did not enter detectors 5 or 6 and thus were incorrectly counted as attenuation events. This correction was calculated using previously measured elastic scattering cross sections [12].

(ii) Charged-particle reaction products, detector 6 correction. All charged-particle reaction products entering detector 6 with energies above the detector 6 threshold (E_{max} − 6.0 MeV) were incorrectly counted as nonattenuation events. This correction was determined by two independent methods.

First, using spectra obtained in the differential cross-section measurements [12], total charged-particle inelastic cross sections from 0 to 6.0 MeV excitation (excluding elastic scattering) were obtained at each incident proton energy and for each nucleus, for scattering angles up to 45°. The correction was calculated by integrating these differential cross sections from 9° (the maximum angle subtended by detector 5) up to 45°.

Second, during each experimental run, in addition to determining the number of attenuation events, pulse height spectra for detector 6 were recorded; specifically, only detector 6 events were recorded which satisfied three criteria: a trigger event $12(\overline{3+4})$ was produced, no signal in detector 5 was detected, and the detector 6 signal was above the (E_{max} − 6.0 MeV) threshold. The net number of events (target in minus target out) below the elastic peak in these spectra were used to determine this correction.

(iii) Charged-particle reaction products, detector 5 correction. All charged particles (including reaction products) entering detector 5 were counted as nonattenuation events. Since the solid angle subtended by detector 5 was small (a cone of half-angle of 9°), the correction was small. This correction (due to the missed reaction products) was estimated using data discussed under the first method of correction (ii) above.

(iv) Nuclear reactions occurring in detector 6. Protons that elastically scattered into detector 6 and that ini-

tiated nuclear reactions in the CsI(Na) scintillator may have been counted as attenuation events. This correction was calculated by using the available data for the reaction probability for a proton stopping in CsI [18]. The number of protons entering detector 6 and missing detector 5 was counted during the experiment for the purpose of this correction.

(v) Detector 5 light guide correction. Detector 5 was a scintillator disk of thickness 0.051 cm imbedded in a flat lucite light guide. A proton elastically scattered from the target and subsequently scattered in the lucite in such a way that it did not enter detector 6 would have produced a false attenuation event. The correction for this effect was calculated using the composition of lucite and the appropriate reaction cross sections [19].

(vi) Other corrections. Other corrections due to target thickness and finite beam spot size were calculated and found to be negligible.

IV. RESULTS AND DISCUSSION

The results for the three nuclei are given in Table II, which includes the major corrections, the final reaction cross sections σ_R, and the associated uncertainties. The uncertainties associated with the uncorrected cross sections are due to statistical fluctuations in the measurements of the attenuation rates with target in and target out, as well as the error associated with the determination of the number of nuclei/cm^2 in the target. The total error in σ_R was obtained by adding all errors in quadrature. The typical error in the final reaction cross sections was 2–3%, except for three of the results for ^{48}Ca, which were between 4.0% and 5.5%.

A. Nuclear transparency calculation

Many of the earlier reaction cross section studies at energies up to 100 MeV were concerned with the behavior of σ_R as a function of mass number at a single energy [14,20–29]. However, more recently there have been a number of experiments which, in addition, have studied the dependence of σ_R on energy [13,15,19,30–37]. Except for heavier nuclei at lower energies where the Coulomb barrier reduces σ_R substantially, the data are well represented at a given energy by a geometrical relation of the form

$$\sigma_R = \pi(r_0 A^{1/3} + \lambda\!\!\!^{-})^2, \tag{1}$$

where r_0 is the radius parameter and $\lambda\!\!\!^{-}$ is the reduced wavelength for the relative motion of the incident proton and target nucleus. It should be noted that r_0 is not entirely energy independent and the above expression does not accurately fit the experimental energy dependence of the total reaction cross section for a particular nucleus over a range of energies for a given r_0. The cross section increases with increasing energy, reaching a broad maximum near 20 MeV, and then slowly decreases, reaching

TABLE II. Proton total reaction cross sections for ^{42}Ca, ^{44}Ca, and ^{48}Ca.

Nucleus	Energy (MeV)	$\sigma_{\text{uncorrected}}$ (mb)	Elastic correction (mb)	Charged-particle reaction products, detector 6 correction (mb)	Charged-particle reaction products, detector 5 correction (mb)	Nuclear reactions in detector 6 correction (mb)	Detector 5 light guide correction (mb)	σ_R (mb)
^{42}Ca	20.8	1134.8±17	−184.7±9	28.9±6	6.9±10	−17.2±1	−3.0±2	966±23
	24.8	1094.0±28	−155.0±8	38.2±8	10.9±10	−17.9±1	−1.2±1	969±32
	29.7	1021.6±22	−121.7±6	40.0±8	13.7±10	−18.5±1	−0.8±1	934±26
	34.8	961.9±21	−91.1±5	47.4±9	18.9±10	−20.4±1	−0.6±1	916±25
	39.7	906.8±14	−64.6±3	51.3±13	23.4±12	−24.0±2	−0.6±1	892±23
	44.9	837.8±14	−40.6±2	44.8±9	22.6±11	−25.3±1	−0.6±1	839±20
	47.8	809.7±14	−28.7±1	44.7±10	24.6±12	−23.5±16	−0.6±1	826±26
^{44}Ca	20.8	1187.3±20	−168.5±8	28.6±6	6.9±10	−17.1±1	−3.0±2	1034±25
	24.8	1142.4±24	−143.3±7	37.1±7	10.6±10	−18.1±1	−1.2±1	1028±28
	29.7	1081.4±20	−114.4±6	40.1±8	13.7±10	−18.4±1	−0.8±1	1002±25
	34.8	997.7±16	−87.1±4	43.7±9	17.5±10	−20.2±1	−0.6±1	951±21
	39.7	952.9±14	−62.6±3	45.0±9	20.5±10	−22.6±1	−0.6±1	933±20
	44.9	876.4±16	−39.5±2	43.9±9	22.1±11	−24.9±1	−0.6±1	877±22
	47.8	869.7±18	−27.3±1	39.2±8	21.6±11	−26.7±4	−0.6±1	876±23
^{48}Ca	23.0	1216.1±41	−152.3±8	7.6±2	6.4±3	−13.8±2	−2.1±1	1062±42
	25.3	1199.7±46	−139.3±7	8.6±2	6.1±3	−15.7±1	−1.2±1	1058±47
	30.3	1117.7±54	−112.5±6	9.9±2	6.6±3	−21.7±4	−0.8±1	999±55
	35.1	1063.4±31	−88.7±4	10.2±2	6.8±3	−20.3±3	−0.6±1	971±32
	39.9	1023.5±30	−65.5±3	9.5±2	6.5±3	−22.6±4	−0.6±1	951±31
	45.3	961.5±33	−41.9±2	7.6±2	6.4±3	−24.9±6	−0.6±1	908±34
	48.0	925.9±19	−30.6±2	6.1±1	5.8±3	−23.7±5	−0.6±1	883±20

a minimum between 100 and 300 MeV.

The energy dependence of σ_R may be represented by a modification of the expression [38,39]

$$\sigma_R = \pi(r_0 A^{1/3} + \lambda)^2 \left[1 - \frac{zZe^2}{(r_0 A^{1/3} + \lambda)E}\right](1 - T), \quad (2)$$

where ze and E are the charge and center of mass energy of the incident particle, Ze is the nuclear charge, and T is the energy dependent nuclear transparency, which can be related to the meanfree path of the incident proton in the target nucleus. Equation (2) represents a more sophisticated way of parametrizing σ_R data with, in effect, the transparency accounting for the difference between the maximum geometrical cross section and the smaller cross section found at higher energies.

Equation (2) was fitted to our experimental σ_R results for ^{42}Ca, ^{44}Ca, and ^{48}Ca. First, the radius parameter r_0 was determined for each nucleus by solving Eq. (2) for r_0 (with $T = 0$) for each experimental σ_R. The maximum calculated value of r_0 was taken to be r_0 for that particular nucleus; these values of r_0 are given in Table III. Then, using these r_0 values and keeping $T = 0$, Eq. (2) was used to calculate the geometrical cross section

TABLE III. Results found with the aid of Eq. (2).

Nucleus	r_0 (fm)	Energy (MeV)	σ_R (Expt.) (mb)	Reference	σ_R [Eq. (2) with $T = 0$] (mb)	T (%)
^{40}Ar	1.56	22.9	1015	[40]	1015	0.0
		28.9	995	[40]	1024	2.8
		35.9	964	[40]	1027	6.1
		42.9	926	[40]	1026	9.7
		46.9	875	[40]	1024	14.6
^{40}Ca		10.34	505	[13]	727	30.5
		11.38	736	[13]	758	2.9
		12.42	730	[13]	783	6.7
		14.97	822	[13]	824	0.3
		15.51	766	[13]	831	7.8
		16.49	765	[13]	841	9.0
	1.47	17.51	850	[13]	850	0.0
		18.54	821	[13]	858	4.3
		19.55	806	[13]	864	6.7
		20.57	851	[13]	869	2.1
		21.59	871	[13]	874	0.3
		24.9	876	[15]	885	1.0
		28.5	913	[14]	892	
		30.0	880	[15]	895	1.7
		35.0	854	[15]	899	5.0
		40.0	807	[15]	901	10.4
		45.0	778	[15]	902	13.7
		48.0	769	[15]	901	14.7
		99.3	580	[23]	888	34.7
^{42}Ca	1.53	20.8	966	this paper	966	0.0
		24.8	969	this paper	978	1.2
		29.7	934	this paper	987	5.7
		34.8	916	this paper	992	7.9
		39.7	892	this paper	994	10.5
		44.9	839	this paper	995	15.9
		47.8	826	this paper	995	17.2
^{44}Ca	1.56	20.8	1034	this paper	1034	0.0
		24.8	1028	this paper	1049	2.0
		29.7	1002	this paper	1059	5.4
		34.8	951	this paper	1064	10.6
		39.7	933	this paper	1066	12.5
		44.9	877	this paper	1066	17.7
		47.8	876	this paper	1066	17.8
^{48}Ca	1.52	23.0	1062	this paper	1062	0.0
		25.3	1058	this paper	1069	1.0
		30.3	999	this paper	1078	7.3
		35.1	971	this paper	1083	10.3
		39.9	951	this paper	1085	12.4
		45.3	908	this paper	1085	16.3
		48.0	883	this paper	1085	18.6

for each energy. These $T = 0$ cross sections are greater than the measured cross sections, as shown in Fig. 2, with the difference increasing with increasing incident proton energy. Equation (2) was next solved for T, using experimental values for σ_R. These results are also listed in Table III.

Also included in Table III and Fig. 2 are results for ^{40}Ar, using experimental results from Ref. [40], and for ^{40}Ca, using experimental results from Refs. [13–15,23]. In the calculation of r_0 for ^{40}Ca, the 13.45, 13.97, and 14.48 MeV data points were ignored, as they exhibit a resonance behavior which cannot be reproduced by Eq. (2).

Each nucleus considered here is completely absorbing ($T = 0$) near 20 MeV incident proton energy and becomes progressively more transparent as the proton energy increases above 20 MeV, with the transparency rising to between 15% and 20% near 50 MeV. This is because the black nucleus cross section ($T = 0$) rises steeply for energies under 20 MeV because of the Coulomb repulsion effect and then becomes almost constant from about 30 to 100 MeV, while the measured reaction cross section falls off steadily for energies above 20 MeV for these A=40–48 nuclei. The smallest radius parameters r_0 occurred for the two doubly magic nuclei ^{40}Ca and ^{48}Ca.

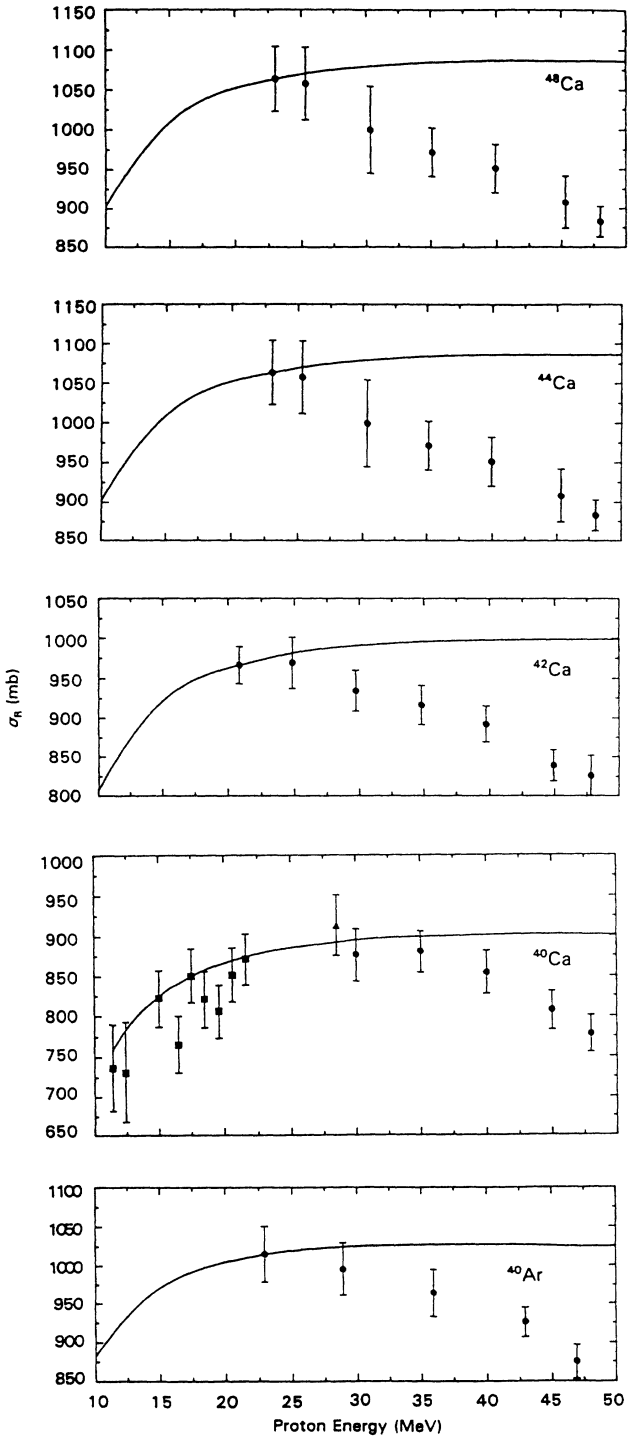

FIG. 2. Plot of σ_R [Eq. (2) with $T = 0$] vs incident proton energy, as given by Table III (solid line) for ^{40}Ar, ^{40}Ca, ^{42}Ca, ^{44}Ca, and ^{48}Ca. Experimental results for each nucleus are also plotted. Legend: •, ^{40}Ar (Ref. [39]); ■, ^{40}Ca (Ref. [13]); ▲, ^{40}Ca (Ref. [14]); •, ^{40}Ca (Ref. [15]); •, ^{42}Ca (this paper); •, ^{44}Ca (this paper); and •, ^{48}Ca (this paper).

B. Optical model analysis

As previously reported [12], the comprehensive set of differential cross sections which were measured for proton elastic scattering from ^{40,42,44,48}Ca between 20 and 49 MeV were analyzed using both a conventional Schrödinger-based optical model and a relativistic opti-

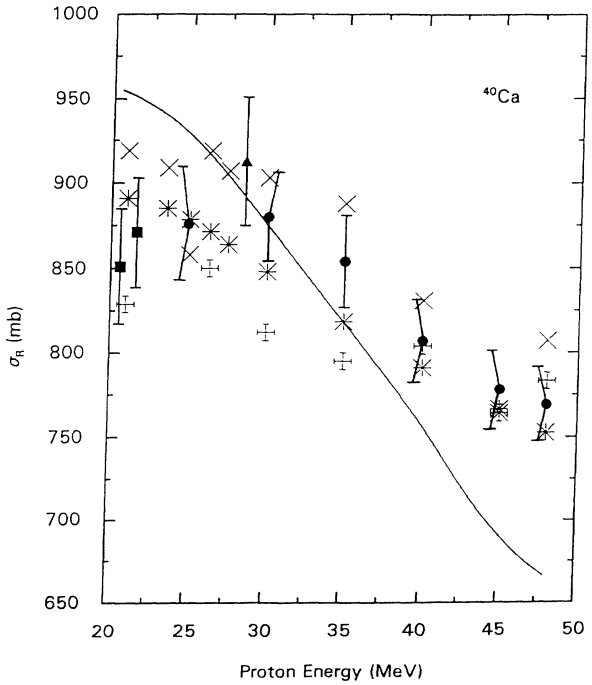

FIG. 3. Optical model predictions for ^{40}Ca. Legend: ×, nonrelativistic optical model results; ⊣⊢, relativistic optical model results; —, global (nonrelativistic) optical model results; and ✳, global (relativistic) optical model results. Experimental results are also included (same legend as in Fig. 2).

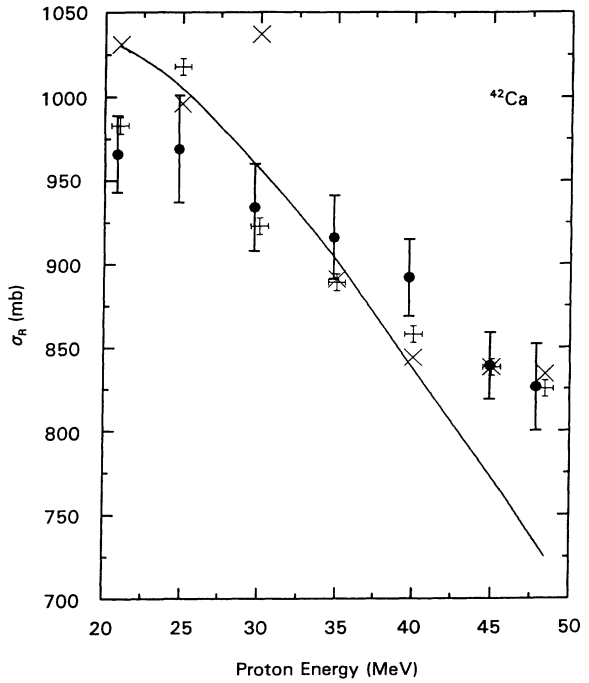

FIG. 4. Optical model predictions for ^{42}Ca. Same legend as for Fig. 3, except that there are no global (relativistic) optical model results.

cal model (Dirac SV model) to enable the extraction of nuclear matter size information on the calcium isotopes. Since experimental σ_R measurements for p+^{40}Ca were available [14,15] prior to this analysis, these data were included in the input to the optical model analysis. The optical model calculations of σ_R for p+^{40}Ca, which are

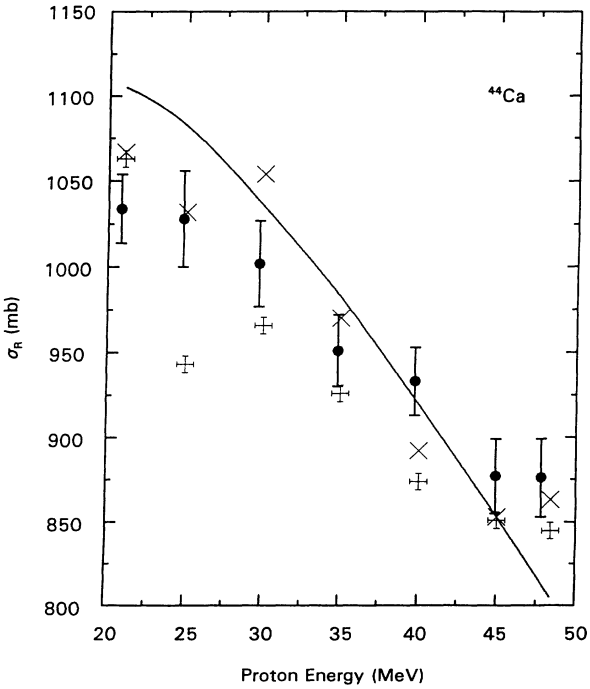

FIG. 5. Optical model predictions for ^{44}Ca. Same legend as for Fig. 4.

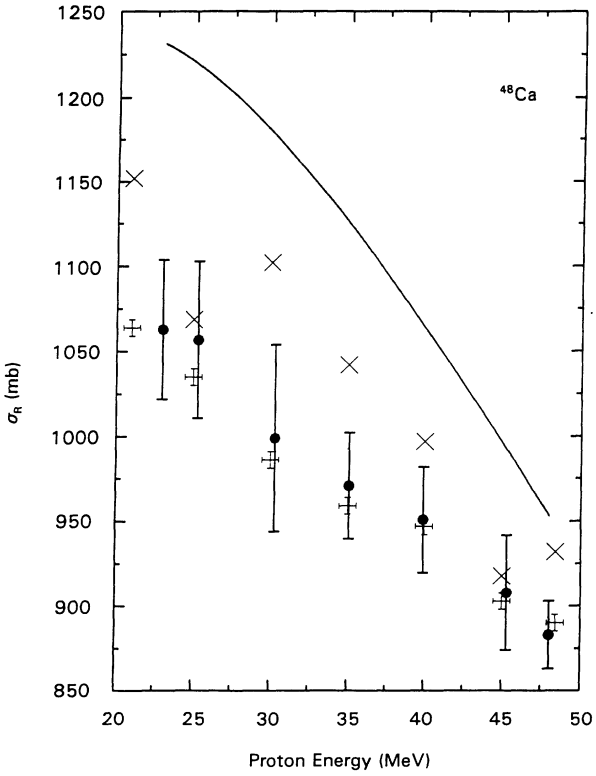

FIG. 6. Optical model predictions for ^{48}Ca. Same legend as for Fig. 4.

the best fit results of the analysis of the elastic scattering data as well as the experimental σ_R data, are shown in Fig. 3. The calculated values can be seen to follow the experimental data quite closely, as expected.

In contrast to the situation for p+^{40}Ca, however, the optical model analysis of the p+^{42,44,48}Ca elastic scattering data preceded the present experimental determination of σ_R for these isotopes. Thus the theoretical σ_R values for p+^{42,44,48}Ca, shown in Figs. 4–6, respectively, are predictions only. Nevertheless, while a certain amount of scatter in the theoretical values is evident, the overall agreement between the experimental and theoretical values is excellent, with a slight overall preference for the relativistic analysis.

C. Comparison with global analysis predictions

Becchetti and Greenlees [41] have analyzed a substantial amount of elastic scattering data for protons with $10 \leq T_p \leq 50$ MeV incident on nuclei with mass numbers $A \geq 40$. They produced a nonrelativistic "global" set of optical model (GOM) parameters. Using their best fit parameters, we have calculated σ_R for protons reacting with the four calcium isotopes studied herein. The results are plotted as a solid line in each of Figs. 3–6 for ^{40,42,44,48}Ca, respectively. The general level of agreement between the GOM predictions and the experimental data is good. For ^{40}Ca, as stated previously [15], the GOM

predictions decrease more rapidly with increasing proton energy than do the experimental values. This same tendency is now observed for ^{42}Ca, ^{44}Ca, and ^{48}Ca. The "intersection energy," where the GOM σ_R prediction is equal to the experimental result, is observed to increase from approximately 30 MeV for ^{40}Ca to 35 MeV for ^{42}Ca and to 40 MeV for ^{44}Ca. However, the GOM result never decreases to the experimental result for ^{48}Ca.

Recently Cooper *et al.* [42] reported results of an energy-dependent global Dirac optical model analysis over a wide energy range (20–1040 MeV). Their results included both energy-dependent A-independent and energy-dependent A-dependent σ_R predictions for ^{40}Ca. One set of predictions, the EDAD fit 1, is identical with previously discussed relativistic optical model fit for ^{40}Ca. In comparing our experimental σ_R results for ^{40}Ca with the four sets of Dirac-based reaction cross section predictions, it is clear that experimental σ_R uncertainties would need to be reduced by a factor of 10 in order to distinguish between the various fits of Ref. [41].

ACKNOWLEDGMENTS

The authors wish to thank Mark McDougall, John Litwin, Paul Beaulieu, Panos Drakopolous, Gerry Maughan, and Lloyd Wheeler for their help in the experimental setup and in data taking, Dan Ifft, Ngyun Bach, Hernawaty Wihjardo, and Lloyd Wheeler for their assistance in the data reduction, and Joel Peavy for his contribution to the preparation of this paper. This work was supported in part by the Research Corporation, the Natural Sciences and Research Council of Canada, and the Faculty Research Committee of the University of Redlands.

[1] B. W. Ridley, University of Colorado Technical Progress Report, 1966 (unpublished).
[2] B. W. Ridley and J. F. Turner, Nucl. Phys. **58**, 497 (1964).
[3] E. E. Gross, R. H. Bassel, L. N. Blumberg, B. J. Morton, A. van der Woude, and A. Zucker, Nucl. Phys. **A102**, 673 (1967).
[4] L. N. Blumberg, E. E. Gross, A. van der Woude, A. Zucker, and R. H. Bassel, Phys. Rev. **147**, 812 (1966).
[5] K. H. Bray, K. S. Jayaraman, G. A. Moss, W. T. H. van Oers, D. O. Wells, and Y. I. Wu, Nucl. Phys. **A167**, 57 (1971).
[6] E. T. Boschitz, R. W. Bereaw, and J. S. Vincent, Phys. Lett. **13**, 322 (1964).
[7] D. L. Watson, J. Lowe, J. C. Dore, R. M. Craig, and D. J. Baugh, Nucl. Phys. **A92**, 193 (1967).
[8] R. M. Craig, J. C. Dore, G. W. Greenlees, J. S. Lilley, and J. Lowe, Nucl. Phys. **58**, 515 (1964).
[9] R. M. Craig, J. C. Dore, J. Lowe, and D. L. Watson, Nucl. Phys. **86**, 113 (1966).
[10] W. T. H. van Oers, Phys. Rev. C **3**, 1550 (1971).
[11] S. M. Austin, E. Kashy, C. H. King, R. G. Markham, I. Redmount, and R. M. Ronnigen, Phys. Rev. C **19**, 1186 (1979).
[12] R. H. McCamis, T. N. Nasr, J. Birchall, N. E. Davison, W. T. H. van Oers, P. J. T. Verheijen, R. F. Carlson, A. J. Cox, B. C. Clark, E. D. Cooper, S. Hama, and R. L. Mercer, Phys. Rev. C **33**, 1624 (1986).
[13] J. F. Dicello, Jr. and G. J. Igo, Phys. Rev. C **2**, 488 (1970).
[14] J. F. Turner, B. W. Ridley, P. E. Cavanagh, G. A. Gard, and A. E. Hardacre, Nucl. Phys. **58**, 509 (1964).
[15] R. F. Carlson, A. J. Cox, J. R. Nimmo, N. E. Davison, S. A. Elbakr, J. L. Horton, A. Houdayer, A. M. Sourkes, W. T. H. van Oers, and D. J. Margaziotis, Phys. Rev. C **12**, 1167 (1975).
[16] B. D. Anderson, P. R. Bevington, F. H. Cverna, M. W. McNaughton, H. B. Willard, R. J. Barrett, N. S. P. King, and D. J. Ernst, Phys. Rev. C **19**, 905 (1979).
[17] R. F. Carlson, W. F. McGill, T. H. Short, J. M. Cameron, J. R. Richardson, W. T. H. van Oers, J. W. Verba, P. Doherty, and D. J. Margaziotis, Nucl. Instrum. Methods **123**, 509 (1975).
[18] A. M. Sourkes, M. S. de Jong, C. A. Goulding, W. T. H. van Oers, E. A. Ginkel, R. F. Carlson, A. J. Cox, and D. J. Margaziotis, Nucl. Instrum. Methods **143**, 589 (1977).
[19] W. F. McGill, R. F. Carlson, T. H. Short, J. M. Cameron, J. R. Richardson, I. Slaus, W. T. H. van Oers, J. W. Verba, D. J. Margaziotis, and P. Doherty, Phys. Rev. C **10**, 2237 (1974).
[20] B. D. Wilkins and G. J. Igo, Phys. Rev. **129**, 2198 (1963).
[21] R. E. Pollock and G. Schrank, Phys. Rev. **140**, B575 (1965).
[22] M. Q. Makino, C. N. Waddell, and R. M. Eisberg, Nucl. Phys. **50**, 145 (1964).
[23] P. Kirby and W. T. Link, Can. J. Phys. **44**, 1847 (1966).
[24] M. Q. Makino, C. N. Waddell, and R. M. Eisberg, Nucl. Phys. **68**, 378 (1965).
[25] R. Goloskie and K. Strauch, Nucl. Phys. **29**, 474 (1962).
[26] K. Bearpark, W. R. Graham, and G. Jones, Nucl. Phys. **73**, 206 (1965).
[27] M. Q. Makino, C. N. Waddell, R. M. Eisberg, and J. Hestenes, Phys. Lett. **9**, 178 (1964).
[28] J. F. Dicello, G. J. Igo, and M. L. Roush, Phys. Rev. **157**, 1001 (1967).
[29] P. J. Bulman and J. A. R. Griffith, Nucl. Phys. **A111**, 315 (1968).
[30] J. J. H. Menet, E. E. Gross, J. J. Malanify, and A. Zucker, Phys. Rev. C **4**, 1114 (1971).
[31] D. G. Montague, R. K. Cole, M. Makino, and C. N. Waddell, Nucl. Phys. **A199**, 457 (1973).
[32] R. F. Carlson, P. Doherty, D. J. Margaziotis, I. Slaus, S. Y. Tin, and W. T. H. van Oers, Lett. Nuovo Cimento **8**, 319 (1973).
[33] I. Slaus, D. J. Margaziotis, R. F. Carlson, W. T. H. van Oers, and J. R. Richardson, Phys. Rev. C **12**, 1093 (1975).
[34] A. M. Sourkes, N. E. Davison, S. A. Elbakr, J. L. Horton, A. Houdayer, W. T. H. van Oers, and R. F. Carlson, Phys. Lett. **51B**, 232 (1974); A. M. Sourkes, A. Houdayer, W. T. H. van Oers, R. F. Carlson, and R. E. Brown, Phys. Rev. C **13**, 451 (1976).

[35] N. E. Davison, D. K. Hasell, A. M. Sourkes, W. T. H. van Oers, R. F. Carlson, and D. J. Margaziotis, Nucl. Phys. **A290**, 45 (1977).
[36] T. N. Nasr, A. M. Sourkes, D. J. Margaziotis, R. F. Carlson, and A. J. Cox, Can. J. Phys. **56**, 56 (1978).
[37] R. Abegg, J. Birchall, N. E. Davison, M. S. de Jong, D. L. Ginther, D. K. Hasell, T. N. Nasr, W. T. H. van Oers, R. F. Carlson, and A. J. Cox, Nucl. Phys. **A324**, 109 (1979).
[38] P. U. Renberg, D. F. Measday, M. Pepin, P. Schwaller, B. Favier, and C. Richard-Serre, Nucl. Phys. **A183**, 81 (1972).
[39] R. M. DeVries and J. C. Peng, Phys. Rev. C **22**, 1055 (1980).
[40] R. F. Carlson, A. J. Cox, T. N. Nasr, M. S. de Jong, D. L. Ginther, D. K. Hasell, A. M. Sourkes, W. T. H. van Oers, and D. J. Margaziotis, Nucl. Phys. **A445**, 57 (1985).
[41] F. D. Becchetti and G. W. Greenlees, Phys. Rev. **182**, 1190 (1969).
[42] E. D. Cooper, S. Hama, B. C. Clark, and R. L. Mercer, Phys. Rev. C **47**, 297 (1993).